

DIRECT SOLUTIONS OF THE MAXWELL EQUATIONS EXPLAIN OPPOSITION PHENOMENA OBSERVED FOR HIGH-ALBEDO SOLAR SYSTEM OBJECTS

MICHAEL I. MISHCHENKO¹, JANNA M. DLUGACH², LI LIU¹, VERA K. ROSENBUSH², NIKOLAI N. KISELEV², AND
 YURI G. SHKURATOV³

¹ NASA Goddard Institute for Space Studies, 2880 Broadway, New York, NY 10025, USA; mmishchenko@giss.nasa.gov

² Main Astronomical Observatory of the National Academy of Sciences of Ukraine, 27 Zabolotny Street, 03680 Kyiv, Ukraine

³ Astronomical Institute of the Kharkiv National University, 35 Sumska Street, 61022 Kharkiv, Ukraine

Received 2009 July 29; accepted 2009 October 2; published 2009 October 20

ABSTRACT

Several spectacular backscattering effects observed for particulate planetary surfaces have been interpreted in terms of the effect of weak localization (WL) of electromagnetic waves. However, the interference concept of WL explicitly relies on the notion of phase of an electromagnetic wave and is strictly applicable only when particles forming the surface are widely separated. Therefore, one needs a definitive quantitative proof of the WL nature of specific optical effects observed for densely packed particulate media. We use numerically exact computer solutions of the Maxwell equations to simulate electromagnetic scattering by realistic models consisting of large numbers of randomly positioned, densely packed particles. By increasing the particle packing density from zero to $\sim 40\%$, we track the onset and evolution of the full suite of backscattering optical effects predicted by the low-density theory of WL, including the brightness and polarization opposition effects (BOE and POE). We find that all manifestations of WL, except the circular polarization ratio and POE, are remarkably immune to packing-density effects. Even POE can survive packing densities typical of planetary regolith surfaces. Our numerical data coupled with the results of unique observations at near-backscattering geometries demonstrate that the BOE and POE detected simultaneously for high-albedo solar system objects are caused by the effect of WL.

Key words: minor planets, asteroids – planets and satellites: individual (Europa) – polarization – radiative transfer – scattering

1. INTRODUCTION

Two spectacular optical phenomena observed simultaneously for a class of high-albedo solar system objects are the brightness and polarization opposition effects (BOE and POE; Rosenbush et al. 2002; Muinonen et al. 2002). The former is a spike-like intensity peak centered at exactly the backscattering direction. The latter is a sharp asymmetric negative-polarization feature with a minimum at a phase angle comparable to the angular semi-width of BOE. It has been suggested that both effects are caused by the effect of weak localization (WL) of electromagnetic waves in particulate media (Mishchenko et al. 2006a and references therein). This interpretation, if correct, could provide specific physical information about the distant objects that would otherwise be difficult to obtain. However, the interference concept of WL explicitly relies on the notion of phase of an electromagnetic wave. As such, it is strictly applicable only when particles forming the scattering medium are widely separated rather than being in direct contact (Barabanenkov et al. 1991; Mishchenko et al. 2006b). Therefore, one needs an unequivocal demonstration of the interference nature of specific backscattering effects observed for planetary regolith surfaces and a definitive proof that WL prevails even when the scattering medium is densely packed.

This demonstration can only be provided by numerically exact computations of electromagnetic scattering by media consisting of large numbers of randomly positioned particles. Indeed, only by directly solving the Maxwell equations can one (1) eliminate any uncertainty associated with the use of an approximate theoretical approach; (2) control precisely all physical parameters of the scattering medium and vary them one at a time; and (3) compute all relevant optical observables at once. As a consequence, one can study the onset,

evolution, and potential decay of all manifestations of WL as the particle packing density gradually increases from zero to values typical of actual particulate surfaces. Such results can provide a definitive answer to the physical origin of BOE and POE as well as explain the peculiar polarized radar returns observed for ice-covered planetary surfaces (Ostro 1993 and references therein). The physically correct interpretation of such backscattering effects is often the only source of information about the composition and microphysical properties of many planetary surfaces.

2. THEORETICAL CONCEPTS

WL (otherwise known as the effect of coherent backscattering (CB)) is a remarkable optical phenomenon which can survive essentially any degree of randomness of particle positions (Barabanenkov et al. 1991; Muinonen 2004; Mishchenko et al. 2006b). The interference origin of WL is illustrated in Figure 1(a) which shows a layer of random particulate medium illuminated by a plane wave incident in the direction $\hat{\mathbf{n}}_{\text{ill}}$ and observed from a very large distance. If the observation direction $\hat{\mathbf{n}}_{\text{obs}}$ is far from the exact backscattering direction given by $-\hat{\mathbf{n}}_{\text{ill}}$, then the average effect of interference of a pair of conjugate scattered waves going through a chain of n particles in opposite directions is zero, owing to the randomness of particle positions. Consequently, the observer measures some average, incoherent intensity. However, when the phase angle α (i.e., the angle between the vectors $\hat{\mathbf{n}}_{\text{obs}}$ and $-\hat{\mathbf{n}}_{\text{ill}}$) is zero, the phase difference between the conjugate paths involving any chain of particles vanishes, and the interference is always constructive.

The most obvious manifestation of WL is a narrow peak of intensity centered at $\alpha = 0^\circ$ (Kuga & Ishimaru 1984; van Albada & Lagendijk 1985; Wolf & Maret 1985). The physical origin of

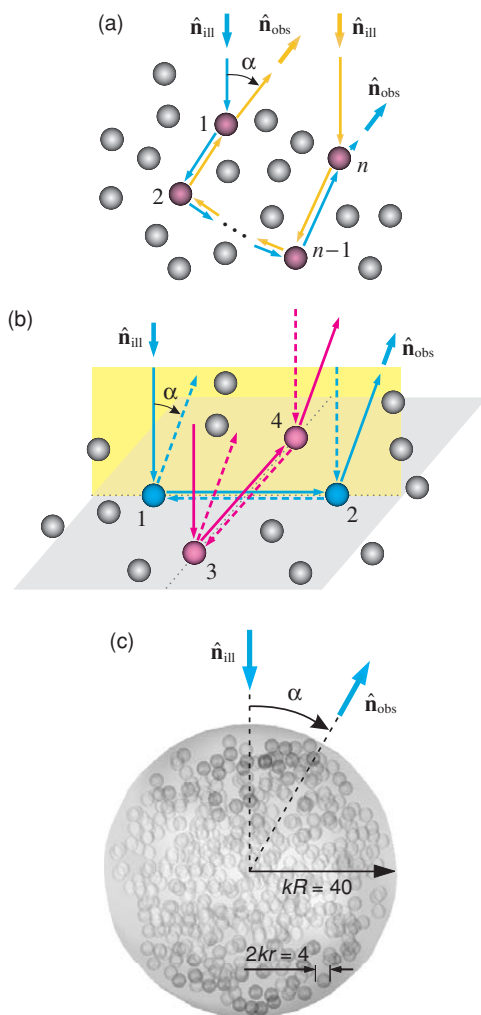


Figure 1. (a) Schematic explanation of WL. The direct (blue arrows) and conjugate (yellow arrows) wave paths go through the same chain of n particles, but in opposite directions. (b) WL origin of POE. Particles 1–4 lie in a plane normal to the scattering plane (shown by yellow). (c) Scattering by a $kR = 40$ spherical volume randomly filled with 500 small ice spheres with $kr = 2$.

a more subtle manifestation of CB is explained in Figure 1(b) (Shkuratov et al. 1994 and references therein). Particles 1–4 lie in a plane normal to the illumination direction and are assumed to have sizes smaller than the wavelength. Particles 1 and 2 lie in the scattering plane (the plane through the illumination and observation directions), while the line through particles 3 and 4 is perpendicular to this plane. If the incident light is unpolarized, then both magenta trajectories yield scattered light polarized negatively with respect to the scattering plane, whereas both blue trajectories yield positively polarized scattered light. The phase difference between the conjugate magenta trajectories is always zero, while that between the blue trajectories is zero at $\alpha = 0^\circ$ but oscillates rapidly with increasing α . Therefore, on average, WL will enhance the negatively polarized scattering trajectories over a wider range of phase angles than the positively polarized trajectories. The result is POE in the form of a negative-polarization minimum at a small α comparable to the angular width of the coherent intensity peak (Mishchenko 1993; Mishchenko et al. 2000). The fact that only certain particle configurations contribute to POE often makes the latter less pronounced than BOE.

The interference concept of WL explicitly relies on assigning a phase to the wave scattered by one particle (e.g., particle 1 in

Figure 1(a)) and exciting another particle (particle 2). However, this implies that particle 2 must be located at a large distance from particle 1, in the so-called far-field zone (Barabanenkov et al. 1991; Mishchenko et al. 2006b). Therefore, one must perform numerically exact computations of electromagnetic scattering directly based on the Maxwell equations in order to determine the range of applicability of the low-packing-density concept of WL to densely packed media in which particles are often in direct contact with each other instead of being separated by large distances.

Such computations have become possible only recently and still require the use of morphologically simplified scattering models (Mishchenko et al. 2007). Specifically, we use the numerically exact T -matrix method (Mackowski & Mishchenko 1996) to compute the scattering of light by a macroscopic volume randomly filled with small ice particles. This model cannot be expected to replicate exactly the diverse morphologies of particulate media formed in varying natural conditions and has practical limitations on the number of constituent particles. However, we will demonstrate that this model affords representative numerical results leading to reliable conclusions.

3. NUMERICALLY EXACT COMPUTER MODELING

Our model of particulate random medium is a spherical volume of radius R filled with N identical non-overlapping spherical particles, Figure 1(c). The size parameter of the volume kR varies from 20 to 50, where k is the wavenumber. The refractive index of the small constituent particles is fixed at a value 1.31 representative of water ice at visible wavelengths. The particle size parameter is also fixed, at a value $kr = 2$. The latter choice is not arbitrary and has the following rationale. Direct computer modeling of POE has been exceedingly difficult (Mishchenko et al. 2007; Petrova et al. 2007) because the polarization of light singly scattered by a particle often has a negative branch at small phase angles (Figure 2). This makes it problematic to distinguish between the singly and multiply scattered negative polarization in a numerical solution of the Maxwell equations. This would not be a problem for particles with size parameters smaller than unity, but their scattering cross section is so small that one would have to use a prohibitively large number of particles to generate a discernable multiple-scattering effect. However, the size parameter $kr = 2$ represents an ideal compromise. Indeed, the scattering cross section for such particles is large enough to cause a significant multiple-scattering component with affordable values of N . Furthermore, the single-scattering polarization for these particles is quite unique in that it has a “shelf” of zero values extending from $\alpha = 0^\circ$ up to 30° (Figure 2), thereby making any multiple-scattering polarization contribution easily identifiable and quantifiable.

We assume that the random particulate volume is illuminated by a quasi-monochromatic beam of light and is observed from a distant point (Figure 1(c)). Using the scattering plane for reference allows us to define the relation between the Stokes parameters of the incident (“inc”) and scattered (“sca”) light in terms of the normalized scattering matrix of the entire volume (Hovenier et al. 2004; Mishchenko et al. 2006b):

$$\begin{bmatrix} I^{\text{sca}} \\ Q^{\text{sca}} \\ U^{\text{sca}} \\ V^{\text{sca}} \end{bmatrix} \propto \begin{bmatrix} a_1(\alpha) & b_1(\alpha) & 0 & 0 \\ b_1(\alpha) & a_2(\alpha) & 0 & 0 \\ 0 & 0 & a_3(\alpha) & b_2(\alpha) \\ 0 & 0 & -b_2(\alpha) & a_4(\alpha) \end{bmatrix} \begin{bmatrix} I^{\text{inc}} \\ Q^{\text{inc}} \\ U^{\text{inc}} \\ V^{\text{inc}} \end{bmatrix}. \quad (1)$$

Depending on kR , the number of constituent particles in Figures 3 and 4 varies from 1 to 600 (see color legends). The

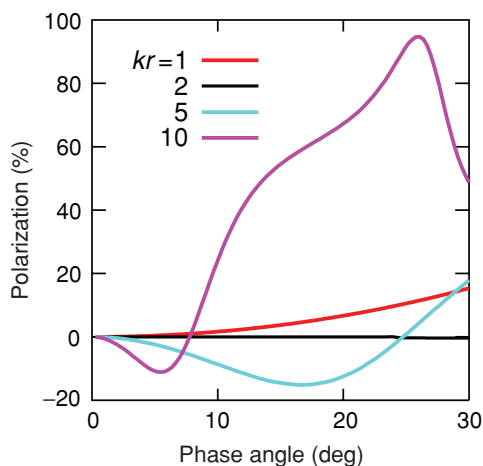


Figure 2. Polarization of scattered light for unpolarized incident light (in percent) vs. phase angle for an ice sphere with a size parameter kr ranging from 1 to 10.

average packing density $\tilde{\rho}$ inside the volume (defined as if the volume were infinite) varies from 1.4% ($N = 10$) to 41.2% ($N = 300$) for $kR = 20$, from 3.6% ($N = 100$) to 21.9% ($N = 600$) for $kR = 30$, and from 1.5% ($N = 100$) to 7.3% ($N = 500$) for $kR = 40$.

Figures 3 and 4 display the most representative numerical results in terms of conventional quantities routinely measured with suitable laboratory and remote-sensing instrumentation such as (polarization) nephelometers, photopolarimeters, and polarization lidars and radars. The phase function $a_1(\alpha)$ characterizes the angular distribution of the intensity scattered by the entire particulate volume provided that the incident light is unpolarized, while the ratio $-b_1(\alpha)/a_1(\alpha)$ gives the corresponding degree of linear polarization. The quantity $\frac{1}{2}(I^{\text{sca}} - Q^{\text{sca}}) \propto \frac{1}{2}[a_1(\alpha) - a_2(\alpha)]$ is relevant to the case of a fully linearly polarized incident light and describes the angular distribution of the intensity component of the scattered light polarized perpendicularly to the incident polarization. If the incident radiation

is fully circularly polarized, then the angular distribution of the scattered intensity component with the same sense of circular polarization is given by $\frac{1}{2}(I^{\text{sca}} + V^{\text{sca}}) \propto \frac{1}{2}[a_1(\alpha) + a_4(\alpha)]$. The linear and circular polarization ratios are defined as the ratio of the cross-polarized to co-polarized scattered intensities and the ratio of the same-helicity to the opposite-helicity scattered intensities, respectively (Ostro 1993). Their respective angular profiles in terms of the scattering matrix elements are given by $\mu_L = [a_1(\alpha) - a_2(\alpha)]/[a_1(\alpha) + 2b_1(\alpha) + a_2(\alpha)]$ and $\mu_C = [a_1(\alpha) + a_4(\alpha)]/[a_1(\alpha) - a_4(\alpha)]$.

4. DISCUSSION

Figure 3 represents the first ever numerically exact display of the most important backscattering effects implied by the approximate theory of WL. Indeed, the normalized scattered intensity $a_1(\alpha)/a_1(0^\circ)$ shows a CB peak rapidly developing with growing N . The peaks in the $\frac{1}{2}(a_1 - a_2)$, $\frac{1}{2}(a_1 + a_4)$, μ_L , and μ_C curves are even more indicative of their multiple-scattering origin since they are absent for a single spherical particle. For the same kR , the angular widths of all these peaks are approximately equal, are independent of N , and are inversely proportional to kR . Since the interference base for finite particulate volumes like that in Figure 1(c) is defined by kR , the above traits testify unequivocally to the interference origin of the backscattering peaks.

The polarization $-b_1(\alpha)/a_1(\alpha)$ is neutral for $N = 1$ but rapidly develops a pronounced minimum with growing N caused by the increasing amount of multiple scattering. It is quite remarkable that the phase angle of minimal polarization, α_{\min} , is virtually independent of N but is inversely proportional to kR , as it should be for POE. Numerical results for $kR = 50$ and N varying from 200 to 600 (not shown here) corroborate the $\alpha_{\min} \propto 1/kR$ trend. Furthermore, α_{\min} is comparable to the angular width of the coherent intensity peak. Finally, the angular shape of the POE minimum is asymmetric, with α_{\min} being significantly smaller than the inversion angle. This behavior is quite different from that exhibited by single-particle

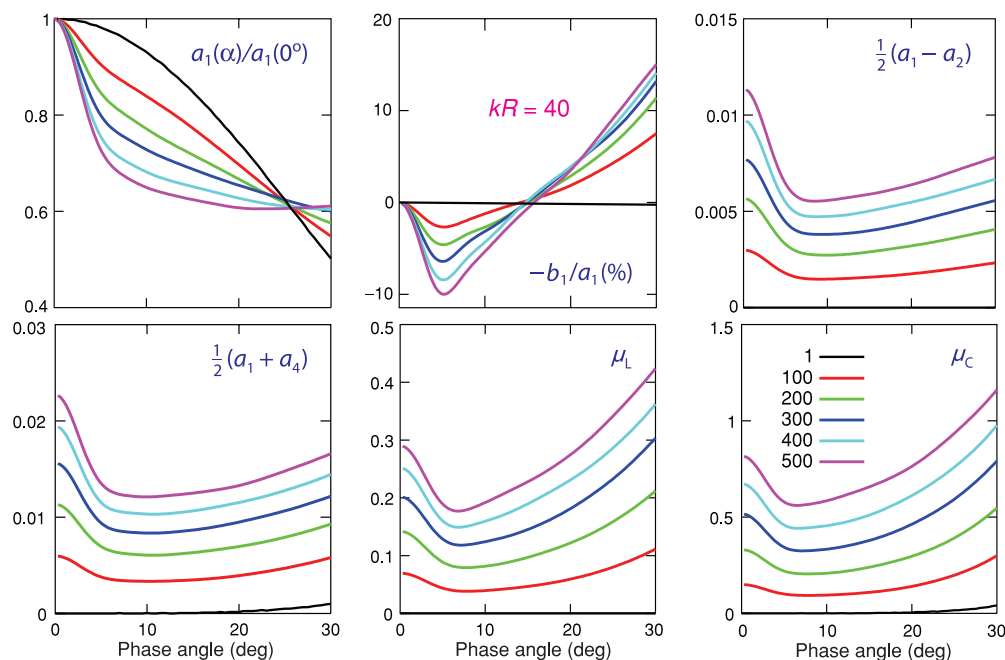


Figure 3. Scattering characteristics of a $kR = 40$ spherical volume randomly filled with small ice spheres and observed from a large distance.

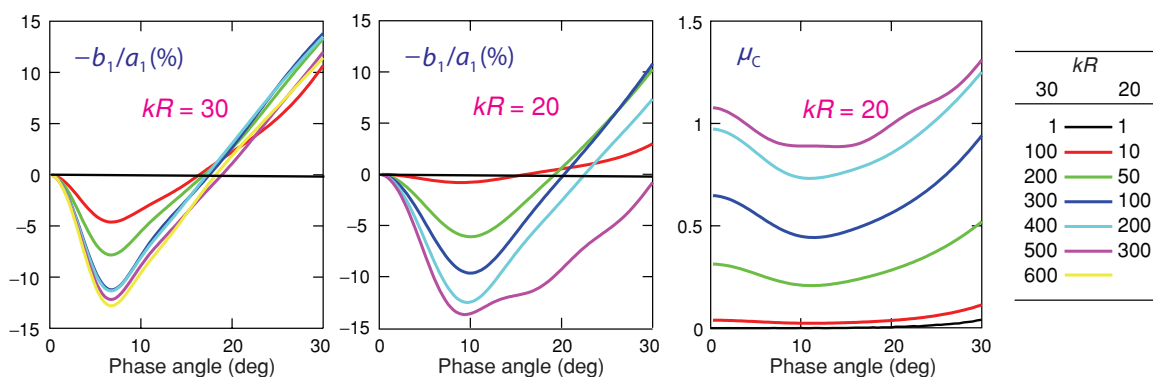


Figure 4. As in Figure 3, but for $kR = 20$ and 30.

negative polarization (Figure 2) but agrees perfectly with the WL prediction (Mishchenko et al. 2000).

All these traits of the backscattering features in Figure 3 prove that they have the common interference origin predicted by the low-packing-density theory of WL. Analogous numerically exact computations for the refractive index 1.5 (representative of mineral particles) fully corroborate this conclusion. They reproduce all potentially observable manifestations of WL (including the POE), each having the same typical angular width and evolving with N according to the theoretical predictions.

Interestingly, Figure 3 shows that depending on the particle microphysical characteristics and the size of the scattering volume, CB can cause a backscattering maximum in the linear polarization ratio μ_L . This numerically exact result demonstrates the limited validity of the previous speculative belief (Hapke 1990; Hapke and Blewett 1991) that CB can only cause a backscattering minimum in μ_L .

The effect of increasing N for a fixed kR is twofold. On the one hand, it causes increased multiple scattering and thereby enhances the classical manifestations of WL. On the other hand, it leads to increased packing density and can cause changes in the backscattering features not predicted by the low-packing-density theory of WL (Tishkovets 2008). Our numerical results in Figures 3 and 4 as well as those not shown here demonstrate that the backscattering peaks in the angular profiles of $a_1(\alpha)/a_1(0^\circ)$, $\frac{1}{2}(a_1 - a_2)$, $\frac{1}{2}(a_1 + a_4)$, and μ_L are remarkably robust and not susceptible to effects of packing density. However, the backscattering peak in μ_C becomes noticeably suppressed when $\tilde{\rho}$ exceeds $\sim 40\%$ (Figure 4). The effect of packing density on POE is also quite significant. Although α_{\min} does not change with $\tilde{\rho}$ (for a fixed kR), the overall shape of the negative polarization minimum changes and the inversion angle shifts toward larger values. This is especially well seen in the results for $kR = 20$. These packing-density effects must be taken into account in the analyses of experimental data.

Our results suggest that the extremely narrow backscattering polarization minimum measured by Lyot 80 years ago for a particulate MgO surface (Lyot 1929) represents the first laboratory observation of POE. Lyot's results were recently reproduced and supplemented by photometric measurements (Shkuratov et al. 2002). The latter revealed an equally narrow backscattering intensity peak, in full agreement with our numerically exact theoretical results.

Our findings are also directly relevant to the explanation of optical opposition phenomena observed for a class of high-albedo solar system objects identified by Mishchenko et al. (2006a). Figure 5 shows the results of observations of the

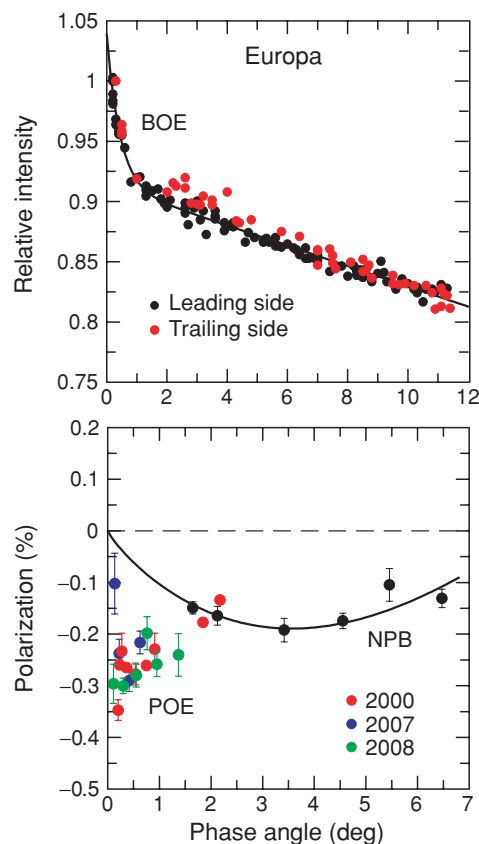


Figure 5. BOE and POE for Europa.

Galilean satellite Europa, which is believed to be covered by almost pure particulate water ice. The upper panel depicts the photometric results from Thompson & Lockwood (1992), while the lower panel combines the results from Rosenbush & Kiselev (2005) and Kiselev et al. (2009) with new 2008 results. The 2000 and 2008 polarimetric data obtained with several spectral filters were averaged according to the procedure described in Rosenbush et al. (2009). It is quite remarkable that Europa exhibits a strong BOE (see also Helfenstein et al. 1998) as well as a pronounced and asymmetric POE. The latter is superposed on a wide, nearly parabolic negative polarization branch (NPB, solid curve) typical of most atmosphereless solar system bodies (Muinonen et al. 2002). Furthermore, the angle of minimal polarization is comparable to the angular semi-width of the backscattering intensity peak.

5. CONCLUDING REMARKS

Virtually all existing measurements of BOE and POE for particulate surfaces are astronomical or laboratory observations rather than controlled laboratory experiments. This means that the particulate surface in question either (1) has a priori unknown properties and (most likely) is highly heterogeneous or (2) is not characterized microphysically in terms of the particle size distribution, shape, refractive index, packing density, and optical thickness. Furthermore, disk-integrated observations of a heterogeneous planetary surface yield a complex convolution of contributions from morphologically different surface types with varying albedos. Some of them can cause BOE and POE of varying angular widths and amplitudes, and some of them can cause only the more robust but still spatially varying BOE. All these factors make it highly problematic to interpret such data unambiguously, especially using direct solutions of the Maxwell equations rather than phenomenological approximation functions (e.g., Hapke 1981) capable of fitting almost any data at the expense of having little or no physical meaning (Mishchenko & Macke 1997).

However, the photometric and polarimetric data for Europa (Figure 5) and several other high-albedo solar system objects (Mishchenko et al. 2006a) are quite unique in that they reveal simultaneous BOE and POE of nearly equal angular widths and with angular profiles consistent with the exact solutions of the Maxwell equations (Figures 3 and 4). No other theory directly based on the Maxwell equations has been demonstrated to yield both effects with their very specific traits simultaneously. Therefore, the results of our theoretical analysis leave little doubt that both opposition effects are caused by the CB of sunlight by a regolith layer composed of microscopic ice grains.

The amplitudes of both observed effects are smaller than those in Figure 3, which could be anticipated. Indeed, it is unlikely that the entire surface of Europa is uniformly covered by the same microscopic grains causing spatially constant BOE and POE. The angular width of the observed BOE and POE is significantly smaller than those in Figure 3, which could also be expected. Indeed, the interference base for a finite scattering volume is controlled by its size parameter kR , whereas that for an optically thick, non-absorbing or weakly absorbing regolith layer is controlled by the transport mean free path (Barabanenkov et al. 1991). The latter can be much greater than the kR values used in our computations, thereby resulting in much narrower opposition effects. The angular profile of the observed polarization at phase angles between 1° and 2° remains poorly defined. As a consequence, it is difficult to infer the packing density of the regolith layer by analyzing the magnitude of packing-density effects. This obviously calls for additional polarimetric observations of Europa whenever suitable observation geometries present themselves.

Undoubtedly, the use of more powerful computers will enable one to explore more sophisticated scattering models consisting of larger numbers of polydisperse particles. In particular, it will be important to analyze the dependence of POE characteristics on the particle size parameter (compared to Geake & Geake 1990) and on the potential presence of absorbing impurities (e.g., Clark 1982), although the latter dependence can be

expected to be relatively weak (Muinonen 2004). Although such modeling will never eliminate the need for advanced laboratory measurements (Gross et al. 2007; Shkuratov et al. 2008), it can be viewed in many respects as an ideal controlled laboratory experiment in which all physical parameters of the scattering medium are known precisely, can be varied one at a time, and can be unambiguously related to specific scattering properties. It can also be expected to provide the ultimate theoretical tool for the interpretation of remote-sensing observations such as the observations of Europa and other high-albedo solar system objects (Rosenbush et al. 2002; Mishchenko et al. 2006b) as well as observations with polarization radars (Ostro 1993; Harmon et al. 1994; Nozette et al. 2001).

This research was funded by the NASA Radiation Sciences Program managed by Hal Maring.

REFERENCES

- Barabanenkov, Yu. N., Kravtsov, Yu. A., Ozrin, V. D., & Saichev, A. 1991, *Prog. Opt.*, **29**, 65
- Clark, R. N. 1982, *Icarus*, **49**, 244
- Geake, J. E., & Geake, M. 1990, *MNRAS*, **245**, 46
- Gross, P., et al. 2007, *Rev. Sci. Instrum.*, **78**, 033105
- Hapke, B. 1981, *J. Geophys. Res.*, **86**, 3039
- Hapke, B. 1990, *Icarus*, **88**, 407
- Hapke, B., & Blewett, D. 1991, *Nature*, **352**, 46
- Harmon, J. K., et al. 1994, *Nature*, **369**, 213
- Helfenstein, P., et al. 1998, *Icarus*, **135**, 41
- Hovenier, J. W., van der Mee, C., & Domke, H. 2004, *Transfer of Polarized Light in Planetary Atmospheres* (Berlin: Springer)
- Kiselev, N., Rosenbush, V., Velichko, F., & Zaitsev, S. 2009, *J. Quant. Spectrosc. Radiat. Transfer*, **110**, 1713
- Kuga, Y., & Ishimaru, A. 1984, *J. Opt. Soc. Am. A*, **1**, 831
- Lyot, B. 1929, *Ann. Obs. Meudon*, **8**, 1
- Mackowski, D. W., & Mishchenko, M. I. 1996, *J. Opt. Soc. Am. A*, **13**, 2266
- Mishchenko, M. I. 1993, *ApJ*, **411**, 351
- Mishchenko, M. I., Liu, L., Mackowski, D. W., Cairns, B., & Videen, G. 2007, *Opt. Express*, **15**, 2822
- Mishchenko, M. I., Luck, J.-M., & Nieuwenhuizen, T. M. 2000, *J. Opt. Soc. Am. A*, **17**, 888
- Mishchenko, M. I., & Macke, A. 1997, *J. Quant. Spectrosc. Radiat. Transfer*, **57**, 767
- Mishchenko, M. I., Rosenbush, V. K., & Kiselev, N. N. 2006a, *Appl. Opt.*, **45**, 4459
- Mishchenko, M. I., Travis, L. D., & Lacis, A. A. 2006b, *Multiple Scattering of Light by Particles* (Cambridge: Cambridge Univ. Press)
- Muinonen, K. 2004, *Waves Random Media*, **14**, 365
- Muinonen, K., et al. 2002, in *Asteroids III*, ed. W. F. Bottke Jr. et al. (Tucson, AZ: Univ. Arizona Press), **123**
- Nozette, S., et al. 2001, *J. Geophys. Res.*, **106**, 23253
- Ostro, S. J. 1993, *Rev. Mod. Phys.*, **65**, 1235
- Petrova, E. V., Tishkovets, V. P., & Jockers, K. 2007, *Icarus*, **188**, 233
- Rosenbush, V. K., & Kiselev, N. N. 2005, *Icarus*, **179**, 490
- Rosenbush, V., Kiselev, N., Avramchuk, V., & Mishchenko, M. 2002, in *Optics of Cosmic Dust*, ed. G. Videen & M. Kocifaj (Dordrecht: Kluwer), **191**
- Rosenbush, V. K., et al. 2009, *Icarus*, **201**, 655
- Shkuratov, Yu. G., Ovcharenko, A. A., Psarev, V. A., & Bondarenko, S. Y. 2008, *Light Scattering Rev.*, **3**, 383
- Shkuratov, Yu. G., et al. 1994, *Earth Moon Planets*, **65**, 201
- Shkuratov, Yu., et al. 2002, *Icarus*, **159**, 396
- Thompson, D. T., & Lockwood, G. W. 1992, *J. Geophys. Res.*, **97**, 14761
- Tishkovets, V. P. 2008, *J. Quant. Spectrosc. Radiat. Transfer*, **109**, 2665
- van Albada, M. P., & Lagendijk, A. 1985, *Phys. Rev. Lett.*, **55**, 2692
- Wolf, P.-E., & Maret, G. 1985, *Phys. Rev. Lett.*, **55**, 2696